

Polymeric Stabilized Emulsions: Steric Effects and Deformation in Soft Systems

Ofer Manor,^{‡,||,¶} Thanh Tam Chau,^{‡,§,||,▽} Geoffrey Wayne Stevens,^{‡,||} Derek Y. C. Chan,^{‡,||,⊥} Franz Grieser,^{§,||} and Raymond Riley Dagastine^{*,‡,||,#}

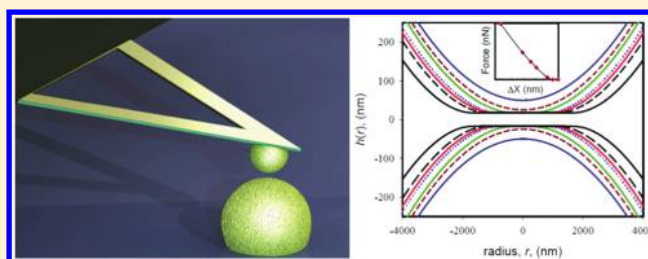
[‡]Department of Chemical and Biomolecular Engineering, [‡]Department of Mathematics and Statistics, [§]School of Chemistry, ^{||}Particulate Fluids Processing Centre, University of Melbourne, Parkville 3010, Australia

[⊥]Faculty of Life and Social Science, Swinburne University of Technology, Hawthorn 3122, Australia

[#]Melbourne Centre for Nanofabrication, 151, Wellington Road, Clayton, 3168, Australia

S Supporting Information

ABSTRACT: Polymeric stabilizers are used in a broad range of processes and products, from pharmaceuticals and engine lubricants to formulated foods and shampoos. In rigid particulate systems, the stabilization mechanism is attributed to the repulsive force that arises from the compression of the polymer coating or “steric brush” on the interacting particles. This mechanism has dictated polymer design and selection for more than thirty years. Here we show, through direct measurement of the repulsive interactions between immobilized drops with adsorbed polymer layers in aqueous electrolyte solutions, that the interaction is a result of both steric stabilization and drop deformation. Drops driven together at slow collision speeds, where hydrodynamic drainage effects are negligible, show a strong dependence on drop deformation instead of brush compression. When drops are driven together at higher collision speeds where hydrodynamic drainage affects the interaction force, simple continuum modeling suggests that the film drainage is sensitive to flow through the polymer brush. These data suggest, for drop sizes where drop deformation is appreciable, that the stability of emulsion drops is less sensitive to the molecular weight or size of the adsorbed polymer layer than for rigid particulate systems.



Polymers are among the most common additives used to control emulsion and foam stability.^{1,2} An understanding of the underlying stabilizing mechanisms operating in these soft matter systems is largely inferred from the effects of polymer additives on the properties of rigid particulate systems. The key thermodynamic theories developed to describe the forces involved in steric stabilization^{1,3} were validated using direct force measurement between two well-defined rigid surfaces. Originally, the surface forces apparatus (SFA)^{4–6} was used with grafted or adsorbed polymer brushes on mica surfaces to study the compression of the polymeric brushes, the influence of flow within the brush,⁷ and lateral shear or frictional behavior.⁷ Later, atomic force microscopy (AFM) was used to extend these studies to a larger range of underlying surfaces including zirconia,⁸ glass,⁹ and hydrophobic substrates.^{10,11} There are few direct measurements of forces in polymer stabilized emulsions¹² and none that have examined the dynamic effects of adsorbed polymers in stabilizing drops or bubbles when the deformation of the interface is significant. With the increasing environmental incentives to process emulsions and foams at low water content and to operate at the edge of stability, it is crucial to gain a more detailed understanding of the role of drop deformation when steric stabilization is in play.

Using an AFM (a MFP-3D, Asylum Research, Santa Barbara, USA) we have measured the dynamic forces during the

controlled collisions between two polymer coated decane drops on the order of 30 to 40 μm in radius. One drop was immobilized on a tipless silicon nitride AFM cantilever (Bruker, Santa Barbara, USA) and the other on a hydrophobic substrate as shown in Figure 1d, where each surface was coated with chromium and gold and then hydrophobised by a monolayer of *n*-octadecane thiol. Each drop has an irreversibly adsorbed¹³ coating of an amphiphilic triblock copolymer of either Pluronic F-108 (Molecular weight: 14 600) or Pluronic P-103 (Molecular weight: 4950), composed of an anchoring block of a propylene oxide (PO) between two ethylene oxide (EO) buoy blocks ((EO)₁₃₂–(PO)₅₆–(EO)₁₃₂ and (EO)₁₇–(PO)₆₀–(EO)₁₇, respectively¹⁴). Any free polymer was removed through solution exchange with 10 mM sodium nitrate electrolyte solutions that also acted to screen electrical double layer forces. The collision velocity was varied by modulating the speed of the AFM piezo actuator on approach and retract. Speeds ranged from 100 nm/s, where dynamic forces such as hydrodynamic drainage are negligible, to 20 to 30 $\mu\text{m/s}$, two to three times faster than the drop velocity moving under

Received: November 1, 2011

Revised: February 16, 2012

Published: February 16, 2012

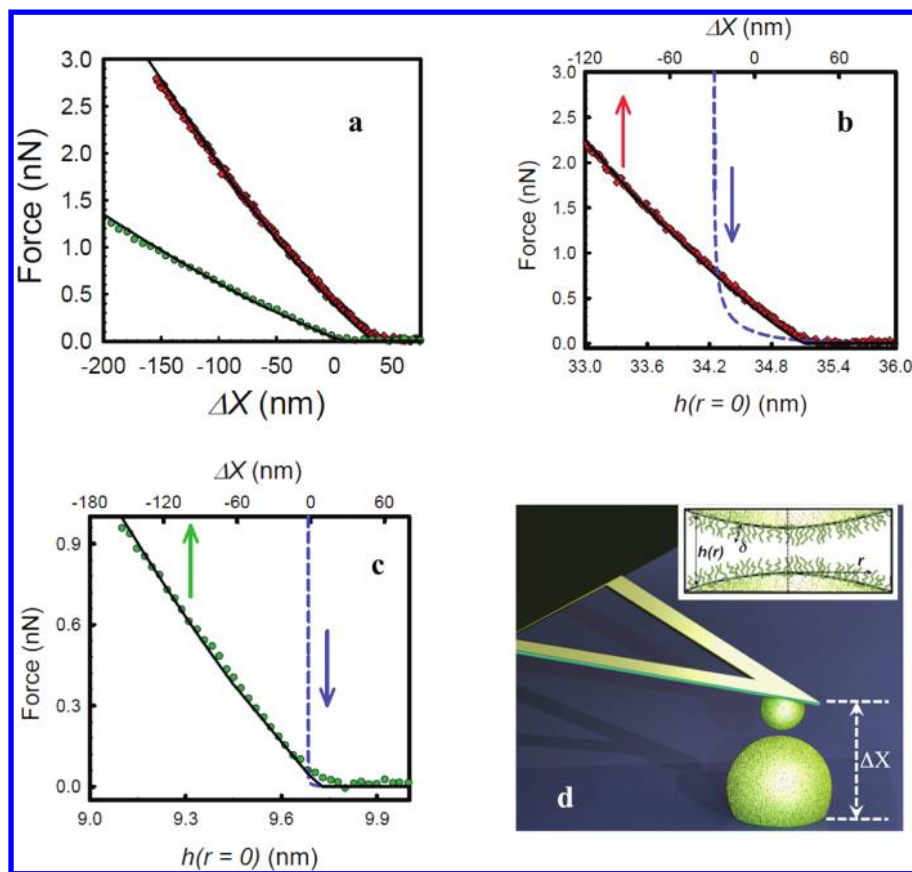


Figure 1. (a) Comparisons between model force calculations (solid lines) and experimental AFM force measurements between two decane droplets in 10 mM sodium nitrate aqueous solutions at an approach velocity of 100 nm/s, coated with steric brushes of Pluronic F-108 (red diamonds) and Pluronic P-103 (green circles). (b) Calculation and measurement of the force between drops coated with F-108 from (a) and the calculated axial separation $h(r=0)$ (dashed line) showing that the change in separation from compression of the polymer brushes is small. The arrows point to the relevant x -axis for each curve. (c) The same calculations as in (b) for drops coated with P-103. (d) Schematic of two polymer coated decane drops in electrolyte solution, where the upper drop is immobilized on an AFM cantilever and the lower drop on a solid substrate. Inset: The intervening thin film between the two drops.

Brownian motion. Further details are discussed in the Supporting Information.

At slow collision velocities, the observed forces between polymer coated drops are strongly repulsive, shown in Figure 1a, as a function of relative piezo displacement, ΔX (defined in Figure 1d), for F-108 and P-103 polymer coated drops. Previous studies of drop interactions have shown that this force is a result of both surface forces and deformation.^{15–18} The surface forces in this system can be attributed to steric forces stabilizing against a van der Waals attraction. Earlier AFM studies on oil drops in the absence of stabilizers have shown that drop coalescence occurs from van der Waals attraction for similar conditions when the drops reach separations of 2 to 5 nm.¹⁸ Thus, the steric force provides a repulsive force that maintains the drops at separations larger than this range.¹⁹

Understanding the impact of interfacial deformation on the forces between the drops requires the interdrop separation, yet this cannot be determined directly from an AFM measurement. To analyze these force data, we employ an existing physical model developed by minimizing the free energy of the drop interfaces to account for local changes of curvature of the interface with the pressures that arise from interaction forces between the drops.^{15,16,20–22} Through this analysis, we are able to link the observed force behavior to the interplay between drop deformation and surface forces in the AFM measurements

for a number of drop^{16–18,23} and bubble systems.^{20,24–26} The incorporation of steric forces and other effects from polymers introduces an added complication. Due to the large number of conformations that are open to the polymer chains, the nature of the oil–solution interface becomes less well-defined, even when monodisperse polymers are adsorbed. Furthermore, the polymers used in this study have significant polydispersity.¹⁴ Thus, applying the AFM analysis methods to a steric system is expected to have inherently more error than simpler systems.

The analysis requires a model calculation of the interfacial profile of the drop on the scale of nanometers. The pressure in this film is then used to calculate a theoretical AFM force as a function of position in the AFM measurement. This theoretical AFM force measurement can then be compared to experimental data.^{15,27} The axi-symmetric geometry of the interface is shown in detail in Figure 1d. The equilibrium polymer brush thickness on each interface is defined by δ . The separation, h , is dependent on radial position, r , as well as time for dynamic forces. In addition, the model requires a set of independently measured parameters including interfacial tension, σ , and geometric parameters (i.e., drop radii, contact angle with the substrate or cantilever) shown in Figure 1, as well as a model for the surface forces between the drops in terms of a disjoining pressure between flat interfaces.¹⁵ In the absence of hydrodynamic drainage, the pressure arises from a

steric force. There are several steric force scaling theories,^{1,3} and we employ the scaling analysis of de Gennes,¹ in which the steric disjoining pressure is given by¹¹

$$\Pi_{\text{steric}} = \alpha \frac{k_B T}{s^3} \left[\left(\frac{2\delta}{h} \right)^{9/4} - \left(\frac{h}{2\delta} \right)^{3/4} \right] \text{ at } 0 < 2\delta < h$$

or $\Pi = 0$ at $2\delta \geq h$ (1)

where $k_B T$ is thermal energy, s is the average distance between contact points on the surface, and α is an empirical parameter from the scaling analysis.²² Several key studies^{10,11} of the forces between adsorbed Pluronic polymers on rigid hydrophobic surfaces offer a baseline set of values for the disjoining pressure parameters. A detailed discussion of the construction of the steric disjoining pressure is included in the Supporting Information.

Comparisons of the experimental force measurements to a theoretical force–distance behavior that accounts for drop deformation and compression of the polymer brushes are shown in Figure 1a. The model calculations employ parameters from the literature or measured independently, summarized in Table 1 and in Table 2. Earlier modeling of AFM force

Table 1. Polymeric Brush Parameters

parameter	P-103 ¹¹	F-108 ¹¹	dynamic theory (F-108)
Polymeric brush thickness, δ	4.8 ± 1 nm	18 ± 2 nm	18 nm
Distance between the coils anchor-sites, s	1.9 ± 0.2 nm	3.7 ± 0.4 nm	3.7 nm
Empirical coefficient, α	0.02	0.07	0.07

Table 2. Experimental Parameters for Pluronic for F-108 and P-103

parameter	P-103	F-108	dynamic theory (F-108)
Viscosity, μ	1 ± 0.2 mPa s	1 ± 0.2 mPa s	1 mPa s
Spring constant, K	0.069 ± 0.010 N/m	0.054 ± 0.008 N/m	0.062 N/m
Interfacial tension, σ	7.4 ± 2 mN/m	14.4 ± 2 mN/m	13.4 mN/m
Drop (on cantilever) radius, R_1	20.6 ± 2.6 μm	23.6 ± 2.6 μm	26.2 μm
contact angle, θ_1	$50 \pm 5^\circ$	$50 \pm 5^\circ$	50°
Drop (on cantilever) radius, R_2	28.7 ± 2.6 μm	33.2 ± 2.6 μm	35.8 μm
contact angle, θ_2	$50 \pm 5^\circ$	$50 \pm 5^\circ$	50°

measurements has shown that the difference in slope is primarily reflective of the difference in interfacial tension when the drops are of similar size. In this case, P-103 is more surface active than F-108 due to the shorter PEO blocks. Using the modeling result, one can compare the changes in axial separation of the drops $h(r=0)$ to the sum of changes in drop deformation and separation, ΔX , and for the same force as shown for the Pluronic F-108 and P-103 coated drops in Figure 1b and c, respectively. Over the observed force range, ΔX varies by several hundred nanometers, yet the change in separation only varies by 1 to 2 nm from the compression of the polymer brushes. For example, the brush layer thickness, δ , for F-108 is 18 nm; thus, the total distance between the oil drops at point of contact between the polymer brushes is 2δ or 36 nm. The closest approach between the drops for the entire force measurement in Figure 1b is 34.2 nm. Thus, the brush

compression is 1.8 nm and the drop deforms instead of the polymer brush with increasing force. This occurs because the steric pressure, Π_{steric} between the drops is bounded by the equivalent Laplace pressure of the interacting drops¹⁵

$$\Delta P = 2\sigma/R \quad (2)$$

where σ is the interfacial tension of the drops and $R = 2/(R_1^{-1} + R_2^{-1})$ is the equivalent radius of the interacting drops with radii R_1 and R_2 . The increased deformation leads to a larger interaction area and thus an increase in the force. This is easily visualized from the interfacial profiles, $h(r)$, from the model calculation shown for the F-108 measurement shown in Figure 2a with a similar result for P-103.

The above analysis demonstrates, not surprisingly, that the drop is the softer object and deforms to a larger extent than the compression of the polymer brush. Thus, provided the range and magnitude of the steric force is larger than that of the van der Waals force, repulsive interactions are expected due to deformation of the drops and not due to increases in repulsive surface forces. This criterion for stability suggests a relative insensitivity to the segment density distribution within the brush and the details of the polymer architecture. The polymers studied, Pluronic F-108 and P-103, have different length PEO blocks but the same PPO moiety, suggesting a lack of sensitivity to polymer molecular weight.

To demonstrate how these effects scale with drop size, we equate the expression of the steric pressure in eq 1 to the Laplace pressure in eq 2. This relation, plotted in Figure 2b for F-108, represents the maximum possible brush compression ($2\delta - h$) achieved during the interaction between two drops as a function of the drop radius. Thus, as the drop radii decrease, the brush compression increases, shown for interfacial tensions ranging from surfactant free interfaces to that of common emulsion systems. The polymer brush compression is still small for drop radii typical for emulsion drops ($<5 \mu\text{m}$) for F-108, but it is the combination of drop radii and interfacial tension, i.e., the Laplace pressure, that will dictate when deformation is no longer critical to the drop interaction. In the limit of large drops or a flat interface, the complex interplay between curvature and the compression of the polymer brush is not expected.²⁸

As the collision velocity increases, hydrodynamic drainage effects become significant and alter the force behavior. For dynamic measurements, the key variable is time. Therefore, it is critical that the force and the piezo actuator motion are recorded with respect to time. Thus, the force versus time is plotted in Figure 3a for approach and retract piezo actuator speeds of 1, 10, and 20 $\mu\text{m/s}$ for the same Pluronic F-108 coated drops studied at slow collision velocities in Figure 1. The piezo actuator moves at an approximately constant velocity during the approach and retract motion for a distance of approximately 2 μm (see Supporting Information). The approach portions of the curves in Figure 3a, the force profile up to the maximum force, show an additional velocity dependent repulsive force; and the retract portions of the curves, the force profile after the maximum force, show a velocity dependent minima that result from the hydrodynamic resistance to the separation of the drops, typical for drop collisions measured using the AFM.^{16,23}

The dynamic drainage force between two drops of this size has been previously described by using a Reynolds lubrication model to describe the flow.^{16,21,22} In this approach, the hydrodynamic pressure is coupled to the drop deformation

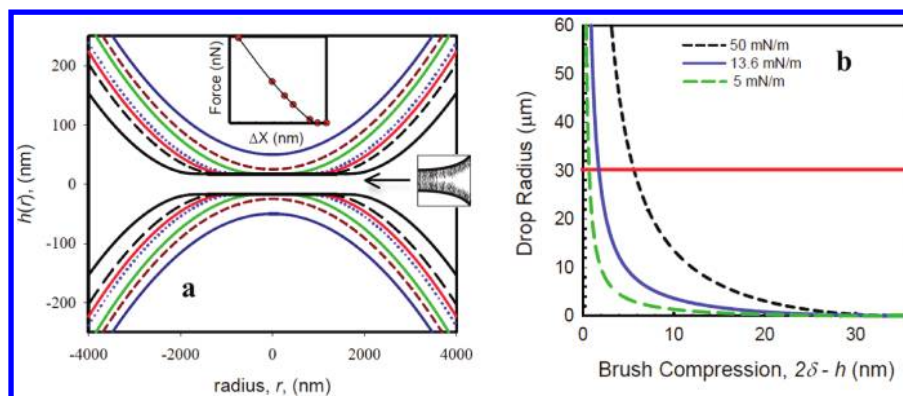


Figure 2. (a) Interfacial profiles, $h(r)$, from the model calculation for the F-108 measurement. The inset is a schematic representation of how the polymer brush has a small overlap or compression region. (b) This correlation illustrates the maximum brush compression ($2\delta - h$) as a function of the drop radius for Pluronic F-108 achieved during a collision for a range of interfacial tensions. Thus, as the radii of the drops decrease, the brush compression increases. This is shown for three interfacial tensions (see legend). The horizontal red line denotes the equivalent Laplace pressure of the drops in this study, indicating little compression of the brush for low interfacial tensions.

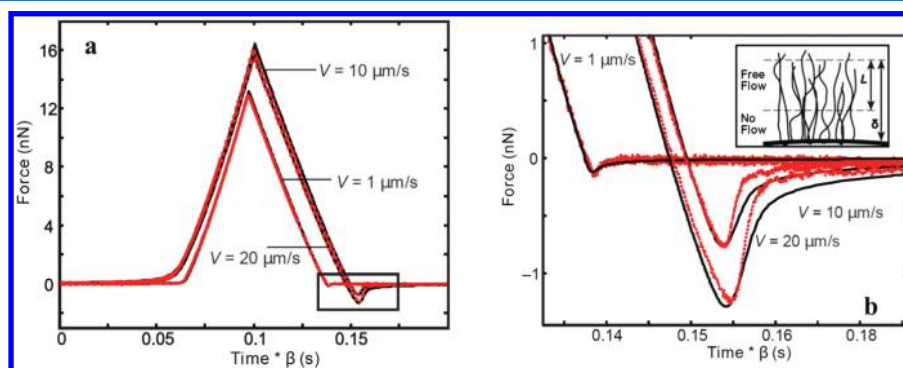


Figure 3. (a) Comparison between the observed dynamic force (red dots) and model calculation (solid line) as a function of time between two colliding decane drops with coatings of Pluronic F-108 at approach and retract piezo actuator speeds 1, 10, and $20 \mu\text{m/s}$. The initial separation for each force measurement $h_{\text{initial}} = 1.95, 2.01, \text{ and } 1.35 \mu\text{m}$, respectively, where the free flow region of the polymer brush was kept constant at $L = 14 \text{ nm}$ for all speeds. The time axis is scaled by a factor β , which is the ratio of the actuator speed of an individual collision to the actuator speed of the fastest collision, 20 mm/s . (b) Enlargement of the box in (a) at the attractive force minima. Inset: a schematic of the flow model through the polymer brush divided into two regions:⁷ a region, $\delta - L$, that does not allow for flow and a region, L , that represents the effective penetration of the aqueous flow into the brush.

described in the static model through the normal stress balance (discussed in the Supporting Information). The existing model assumes a simple interface where an adsorbed polymer layer is more complex. The aqueous flow in the brush is accounted for using a simplified model by Klein.⁷ The polymer brush is divided into two regions: one region where there is free flow through the brush, defined by L , and the second region, where there is no flow within the polymer brush, defined by thickness $\delta - L$, as shown in the inset in Figure 3b. In addition, the boundary of the region between flow and no flow is assumed to provide a tangentially immobile surface for the hydrodynamic boundary condition at the interface (i.e., assuming no internal flow in the drops, previously observed for a number of drops measurements in the absence and presence of surfactants^{16–18}).

Figure 3a and b shows the comparison between the experimental data and theoretical calculation where the region of fluid flow in each polymer brush is 14 nm out of a possible 18 nm . The input parameters are summarized in Table 1 and Table 2. The thickness of the region of the polymer brush with free fluid flow was the same for all velocities; thus, the agreement with the data and the fact that the magnitude of L is independent of the collision speeds studied suggests a consistent description of the flow through the brush. Sensitivity

studies of these data, discussed in the Supporting Information, suggest that the accuracy of L is limited by the experimental error in the estimates of δ and the fact that this model is simplistic and neglects the details of the polymer segment density extending from the oil–water interface.

The dynamic behavior is similar to the case of no hydrodynamic drainage in several ways. Again, the slope of the force curve at small separations corresponds to higher forces and is proportional to the interfacial tension.²² Snapshots of calculated interfacial profiles, similar to the plot in Figure 2a, for the $20 \mu\text{m/s}$ drop collision show the interface flattening to a film thickness of 34.2 nm , similar to the slow collision case. Aspects unique to the dynamic nature of the interaction are based around flow through the polymer brush. The effect of the polymer brush becomes more pronounced as the film thickness between the brushes decreases and the flow through the brush becomes a larger fraction of the total drainage volume. This occurs at low to moderate forces on the approach and in the minima on the retraction of the force versus time curves, leading to a substantial influence on the hydrodynamic drainage behavior. Although this model was sufficient to describe the drainage behavior between the drops, it is unlikely that this simplistic model can capture all the details of flow through the

brush. Regardless, the deformation of the drop is still an important aspect for both the static and dynamic cases.

The interplay between drop deformation and compression of the adsorbed polymer brush indicates that for sufficiently large drop radii or, more accurately, for sufficiently low Laplace pressures, deformation can play a larger role than steric forces in repulsive drop interactions or emulsion stability. For the polymer and drop sizes studied, the outcome appears insensitive to the molecular weight affect on the steric force. This also suggests that the stability of an emulsion drop of micrometer size or larger may be insensitive to the polymer architecture as well. In addition, the drop deformation is equally important in the dynamic interactions between drops where the volume of aqueous flow through the brush also affects the dynamic interactions.

These results demonstrate the importance of rigidity of the underlying material in soft matter systems when compressing a steric polymer brush. This is also applicable to living cells, for example, in the analysis of recent studies on the polymer brush layers native to cancer cells.²⁹ Here, similarly, the stiffness of the underlying material (in this case a cancer cell with stiffness of $\sim 2\text{--}4$ kPa²⁹) is significantly smaller than expected from steric pressures that arise from compression of a polymer brush. Thus, in a direct force measurement such as the AFM, deformation of the cell would be expected instead of compression of the steric brush; therefore, caution should be used in any analysis that neglects cellular deformation.

■ ASSOCIATED CONTENT

📄 Supporting Information

Details of experimental procedures, materials and modeling are included. This material is available free of charge via the Internet at <http://pubs.acs.org>.

■ AUTHOR INFORMATION

Corresponding Author

*E-mail: rrd@unimelb.edu.au.

Present Addresses

[¶]School of Electrical and Computer Engineering, RMIT, Melbourne 3001, Australia

[▽]IP Australia, 658 Church street, Richmond VIC 3121, Australia

Notes

The authors declare no competing financial interest.

■ ACKNOWLEDGMENTS

The ARC is thanked for financial support, and the Particulate Fluids Processing Centre for infrastructure support for the project. R. Tabor is thanked for useful discussions.

■ REFERENCES

- (1) de Gennes, P. G. Polymers at an interface - a simplified view. *Adv. Colloid Interface Sci.* **1987**, *27*, 189–209.
- (2) Israelachvili, J. N. *Intermolecular and surface forces*, 2nd ed.; Academic Press Limited: San Diego, 1991.
- (3) Milner, S. T.; Witten, T. A.; Cates, M. E. Theory of the grafted polymer brush. *Macromolecules* **1988**, *21*, 2610–2619.
- (4) Hadziioannou, G.; Patel, S.; Granick, S.; Tirrell, M. Forces between surfaces of block copolymers adsorbed on mica. *J. Am. Chem. Soc.* **1986**, *108*, 2869–2876.
- (5) Klein, J. Forces between 2 polymer layers adsorbed at a solid-liquid interface in a poor solvent. *Adv. Colloid Interface Sci.* **1982**, *16*, 101–115.

(6) Klein, J.; Kamiyama, Y.; Yoshizawa, H.; Israelachvili, J. N.; Fredrickson, G. H.; Pincus, P.; Fetters, L. J. Lubrication forces between surfaces bearing polymer brushes. *Macromolecules* **1993**, *26*, 5552–5560.

(7) Klein, J. Shear, friction, and lubrication forces between polymer-bearing surfaces. *Annu. Rev. Mater. Sci.* **1996**, *26*, 581–612.

(8) Biggs, S. Steric and bridging forces between surfaces bearing adsorbed polymer - an atomic-force microscopy study. *Langmuir* **1995**, *11*, 156–162.

(9) Braithwaite, G. J. C.; Howe, A.; Luckham, P. F. Interactions between poly(ethylene oxide) layers adsorbed to glass surfaces probed by using a modified atomic force microscope. *Langmuir* **1996**, *12*, 4224–4237.

(10) McLean, S. C.; Lioe, H.; Meagher, L.; Craig, V. S. J.; Gee, M. L. Atomic force microscopy study of the interaction between adsorbed poly(ethylene oxide) layers: Effects of surface modification and approach velocity. *Langmuir* **2005**, *21*, 2199–2208.

(11) Musoke, M.; Luckham, P. E. Interaction forces between polyethylene oxide-polypropylene oxide ABA copolymers adsorbed to hydrophobic surfaces. *J. Colloid Interface Sci.* **2004**, *277*, 62–70.

(12) Mondain-Monval, O.; Espert, A.; Omarjee, P.; Bibette, J.; Leal-Calderon, F.; Philip, J.; Joanny, J. F. Polymer-induced repulsive forces: Exponential scaling. *Phys. Rev. Lett.* **1998**, *80*, 1778.

(13) Svitova, T. F.; Radke, C. J. AOT and pluronic F68 coadsorption at fluid/fluid interfaces: A continuous-flow tensiometry study. *Ind. Eng. Chem. Res.* **2005**, *44*, 1129–1138.

(14) Baker, J. A.; Berg, J. C. Investigation of the adsorption configuration of poly(ethylene oxide) and its copolymers with poly(propylene oxide) on model polystyrene latex dispersions. *Langmuir* **1988**, *4*, 1055–1061.

(15) Chan, D. Y. C.; Dagastine, R. R.; White, L. R. Forces between a rigid probe particle and a liquid interface I. The repulsive case. *J. Colloid Interface Sci.* **2001**, *236*, 141–154.

(16) Dagastine, R. R.; Manica, R.; Carnie, S. L.; Chan, D. Y. C.; Stevens, G. W.; Grieser, F. Dynamic forces between two deformable oil droplets in water. *Science* **2006**, *313*, 210–213.

(17) Dagastine, R. R.; Webber, G. B.; Manica, R.; Stevens, G. W.; Grieser, F.; Chan, D. Y. C. Viscosity effects on hydrodynamic drainage force measurements involving deformable bodies. *Langmuir* **2010**, *26*, 11921–11927.

(18) Lockie, H. J.; Manica, R.; Stevens, G. W.; Grieser, F.; Chan, D. Y. C.; Dagastine, R. R. Precision AFM measurements of dynamic interactions between deformable drops in aqueous surfactant and surfactant-free solutions. *Langmuir* **2011**, *27*, 2676–2685.

(19) Bevan, M. A.; Prieve, D. C. Forces and hydrodynamic interactions between polystyrene surfaces with adsorbed PEO-PPO-PEO. *Langmuir* **2000**, *16*, 9274–9281.

(20) Tabor, R. F.; Chan, D. Y. C.; Grieser, F.; Dagastine, R. R. Anomalous stability of carbon dioxide in pH-controlled bubble coalescence. *Angew. Chem.* **2011**, *123*, 3516–3518.

(21) Carnie, S. L.; Chan, D. Y. C.; Lewis, C.; Manica, R.; Dagastine, R. R. Measurement of dynamical forces between deformable drops using the atomic force microscope. I. Theory. *Langmuir* **2005**, *21*, 2912–2922.

(22) Manica, R.; Connor, J. N.; Dagastine, R. R.; Carnie, S. L.; Horn, R. G.; Chan, D. Y. C. Hydrodynamic forces involving deformable interfaces at nanometer separations. *Phys. Fluids A* **2008**, *20*, 032101.

(23) Webber, G. B.; Edwards, S. A.; Stevens, G. W.; Grieser, F.; Dagastine, R. R.; Chan, D. Y. C. Measurements of dynamic forces between drops with the AFM: Novel considerations in comparisons between experiment and theory. *Soft Matter* **2008**, *4*, 1270–1278.

(24) Vakarelski, I. U.; Manica, R.; Tang, X. S.; O'Shea, S. J.; Stevens, G. W.; Grieser, F.; Dagastine, R. R.; Chan, D. Y. C. Dynamic interactions between microbubbles in water. *Proc. Natl. Acad. Sci. U. S. A.* **2010**, *107*, 11177–11182.

(25) Tabor, R. F.; Manica, R.; Chan, D. Y. C.; Grieser, F.; Dagastine, R. R. Repulsive van der Waals forces in soft matter: Why bubbles do not stick to walls. *Phys. Rev. Lett.* **2011**, *106*, 064501.

(26) Manor, O.; Vakarelski, I. U.; Tang, X.; O'Shea, S. J.; Stevens, G. W.; Grieser, F.; Dagastine, R. R.; Chan, D. Y. C. Hydrodynamic boundary conditions and dynamic forces between bubbles and surfaces. *Phys. Rev. Lett.* **2008**, *101*, 024501/1–024501/4.

(27) Dagastine, R. R.; Prieve, D. C.; White, L. R. Forces between a rigid probe particle and a liquid interface. III. Extraction of the planar half-space interaction energy $E(D)$. *J. Colloid Interface Sci.* **2004**, *269*, 84–96.

(28) Gotchev, G.; Kolarov, T.; Khristov, K.; Exerowa, D. Electrostatic and steric interactions in oil-in-water emulsion films from pluronic surfactants. *Adv. Colloid Interface Sci.* **2011**, *168*, 79–84.

(29) Iyer, S.; Gaikwad, R. M.; Subba Rao, V.; Woodworth, C. D.; Sokolov, I. Atomic force microscopy detects differences in the surface brush of normal and cancerous cells. *Nat. Nano* **2009**, *4*, 389–393.